STRUCTURAL BIOLOGY COMMUNICATIONS

ISSN 2053-230X

# The structure of the death receptor 4–TNF-related apoptosis-inducing ligand (DR4–TRAIL) complex

Vidhyashankar Ramamurthy,[a] Aaron P. Yamniuk,[b] Eric J. Lawrence,[b] Wei Yong,[a] Lumelle A. Schneeweis,[b] Lin Cheng,[b] Melissa Murdock,[b] Martin J. Corbett,[b] Michael L. Doyle[b] and Steven Sheriff[a]*

[a]Molecular Structure and Design, Bristol-Myers Squibb R&D, PO Box 4000, Princeton, NJ 08543-4000, USA, and [b]Protein Science, Bristol-Myers Squibb R&D, PO Box 4000, Princeton, NJ 08543-4000, USA. *Correspondence e-mail: steven.sheriff@bms.com

Received 14 July 2015
Accepted 2 September 2015

Edited by H. M. Einspahr, Lawrenceville, USA

**Keywords:** death receptor 4; death receptor 5; TNF-related apoptosis-inducing ligand.

**PDB reference**: DR4–TRAIL complex, 5cir

**Supporting information**: this article has supporting information at journals.iucr.org/f

The structure of death receptor 4 (DR4) in complex with TNF-related apoptosis-inducing ligand (TRAIL) has been determined at 3 Å resolution and compared with those of previously determined DR5–TRAIL complexes. Consistent with the high sequence similarity between DR4 and DR5, the overall arrangement of the DR4–TRAIL complex does not differ substantially from that of the DR5–TRAIL complex. However, subtle differences are apparent. In addition, solution interaction studies were carried out that show differences in the thermodynamics of binding DR4 or DR5 with TRAIL.

## 1. Introduction

Apoptosis is the process of controlled, programmed cell death. It is critical for normal tissue development and homeostasis. TNF-related apoptosis-inducing ligand (TRAIL) is a cytokine that can trigger apoptosis in cancer cell lines and is therefore of current interest as a cancer therapy. TRAIL is a 281-residue type II transmembrane protein and forms stable homotrimers both on the cell surface and in its proteolytically generated soluble shed form (van Roosmalen *et al.*, 2014). The X-ray crystallographic structure of TRAIL has been reported (Hymowitz *et al.*, 2000). TRAIL binds to five known receptors: death receptor 4 (DR4), death receptor 5 (DR5), decoy receptor 1 (DcR1), decoy receptor 2 (DcR2) and osteoprotegerin (OPG) (Truneh *et al.*, 2000). The biological response to TRAIL is tissue-dependent, and is likely to depend on the expression levels of TRAIL and its receptors, the affinities and kinetics of the TRAIL–receptor interactions and possible combinatorial interactions with various different receptors.

There are a number of agents targeting the TRAIL receptors as anticancer agents (Stuckey & Shah, 2013; Prasad *et al.*, 2014). Both DR4 and DR5 are expressed on cancer cells and are known to be involved in apoptosis, yet it is not well understood why both death receptors exist or if selectively targeting one over the other will lead to an improved therapeutic profile (van Roosmalen *et al.*, 2014). The X-ray crystallographic structure of the TRAIL–DR5 complex has been reported (Hymowitz *et al.*, 2000; Mongkolsapaya *et al.*, 1999; Cha *et al.*, 2000). In contrast, the X-ray crystallographic structure of the TRAIL–DR4 complex has not been reported. In order to understand the functional differences between TRAIL binding to DR5 *versus* DR4, we report here the first

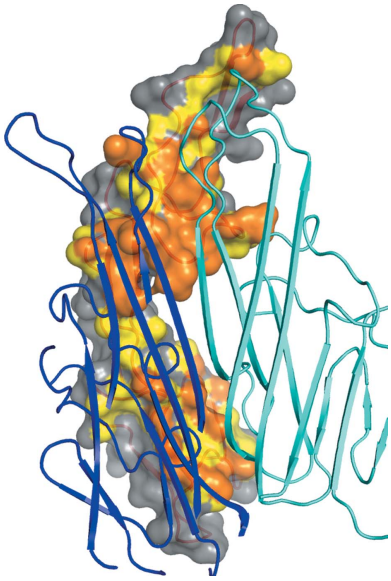

**Table 1**
Macromolecule-production information.

| | DR4 | DR5 | TRAIL |
|---|---|---|---|
| Source organism | *Homo sapiens* | *Homo sapiens* | *Homo sapiens* |
| DNA source | BMS cDNA collection | BMS cDNA collection | BMS cDNA collection |
| Forward primer | NdeI/$His_6$ tag | NdeI/$His_6$ tag | NcoI |
| Reverse primer | XhoI | XhoI | XhoI |
| Cloning vector | pET-28-NM | pET-28-NM | pET-28-Nhis-TEV |
| Expression host | *E. coli* | *E. coli* | *E. coli* |
| Complete amino-acid sequence of the construct produced | MHHHHHHATIKLHDQSIGTQQWEHSPLGELC-PPGSHRSERPGACNRCTEGVGYTNASNNL-FACLPCTACKSDEEERSPCTTTRNTACQC-KPGTFRNDNSAEMCRKCSTGCPRGMVKVK-DCTPWSDIECVHKESGNG | MHHHHHHALITQQDLAPQQRAAPQQKRSSPS-EGLCPPGHHISEDGRDCISCKYGQDYSTH-WNDLLFCLRCTRCDSGEVELSPCTTTRNT-VCQCEEGTFREEDSPEMCRKCRTGCPRGM-VKVGDCTPWSDIECVHKES | MVRERGPQRVAAHITGTRGRSNTLSSPNSKN-EKALGRKINSWESSRSGHSFLSNLHLRNG-ELVIHEKGFYYIYSQTYFRFQEEIKENTK-NDKQMVQYIYKYTSYPDPILLMKSARNSC-WSKDAEYGLYSIYQGGIFELKENDRIFVS-VTNEHLIDMDHEASFFGAFLVG |

X-ray crystallographic structure of the complex of soluble human TRAIL bound to soluble human DR4. We have also conducted solution interaction studies of soluble TRAIL with soluble forms of DR5 and DR4 to understand the differences between the interaction of TRAIL with these receptors.

## 2. Materials and methods

### 2.1. Macromolecule production

The genes for the coding regions of N-terminally His-tagged DR4, N-terminally His-tagged DR5 and TRAIL were generated by the PCR reaction using a template from the BMS cDNA collection. For DR4 and DR5, DNA fragments were then subcloned into pET-28-NM vector using NdeI and XhoI restriction sites. The TRAIL DNA fragment was subcloned into pET-28-Nhis-TEV vector using NcoI and XhoI sites.

The recombinant pET-28 plasmid containing the DR4 gene of interest with an N-terminal His tag (Table 1) was transformed into *Escherichia coli* Origami B (DE3) cells for expression. For expression, the transformed cells were grown at 37°C with shaking at 250 rev $min^{-1}$ until the $OD_{600\ nm}$ reached ∼0.6, when the temperature was reduced to 15°C and the cells were allowed to equilibrate. IPTG was then added to a final concentration of 1 m*M* and the cells were allowed to grow overnight at 15°C with shaking at 250 rev $min^{-1}$.

For the purification of DR4, ∼35 g of overexpressed cells obtained as above were resuspended in 150 ml lysis buffer (50 m*M* $NaH_2PO_4$, 300 m*M* NaCl, 10 m*M* imidazole pH 8.0). Two tablets of cOmplete EDTA-free protease inhibitor (Sigma-Aldrich), 10 mg DNAse I and 2 m*M* $MgCl_2$ were added to the above mixture. The cells were lysed using an Avestin emulsifier and the lysate was centrifuged at 14 500 rev $min^{-1}$ (Sorvall SS34 rotor) for 30 min at 4°C. 10 ml Ni–NTA Superflow resin suspension was added to the supernatant and mixed for 1 h at 4°C. The mixture was then packed onto a column and the flowthrough (FT) was collected. The column was subsequently washed with 50 ml wash buffer 1 (50 m*M* $NaH_2PO_4$, 300 m*M* NaCl, 20 m*M* imidazole pH 8.0) and the wash (W1) was collected. The column was then washed with 25 ml wash buffer 2 (50 m*M* $NaH_2PO_4$, 300 m*M* NaCl, 40 m*M* imidazole pH 8.0) and the wash (W2) was collected. Elution was carried out with 10 × 5 ml elution buffer (50 m*M* $NaH_2PO_4$, 300 m*M* NaCl, 500 m*M* imidazole pH 8.0) and eluates E1–E10 were collected. Subsequently, eluates E1–E9 were combined and desalted to remove the imidazole. This sample was then subjected to further purification on a 4 ml Ni–NTA Superflow resin column equilibrated with 50 m*M* $NaH_2PO_4$, 300 m*M* NaCl, 10 m*M* imidazole pH 8.0. The bound protein was then eluted using 50 m*M* $NaH_2PO_4$, 300 m*M* NaCl, 500 m*M* imidazole pH 8.0 by employing a 20 column-volume gradient. The purification procedure for DR5 was identical.

The human TRAIL plasmid was transformed into *E. coli* BL21 (DE3) host cells and selected for kanamycin resistance on LB plates with 50 µg $ml^{-1}$ kanamycin. Shake flasks of LB containing 50 µg $ml^{-1}$ kanamycin were inoculated with a 1:100 dilution of starter culture at an $OD_{600\ nm}$ of 0.4, grown for 3 h at 37°C until an $OD_{600\ nm}$ of 1.3 was achieved and induced with 1 m*M* IPTG at a decreased temperature of 20°C for 18 h. The cell pellets were harvested by centrifugation and stored frozen at −80°C until processed. The cell pellets were resuspended by agitation in lysis buffer [20 m*M* Tris–HCl pH 7.5, 10 m*M* EDTA, 150 m*M* NaCl, 1.0% Triton X-100, 1× Protease Inhibitor Cocktail Set V, EDTA-free (Calbiochem), 2.5 units $ml^{-1}$ Benzonase (Novagen)] at 10:1(*w*:*v*). The sample was processed with a Panda (Niro Soavi) benchtop high-pressure homogenizer at a pressure of 80 MPa. The lysate was centrifuged at 15 000*g* for 30 min and the inclusion bodies were washed with wash buffer *A* (20 m*M* Tris–HCl pH 7.5, 10 m*M* EDTA, 150 m*M* NaCl, 0.5% Triton X-100) at 20:1(*w*:*v*). Inclusion bodies were isolated by centrifugation and washed with wash buffer *B* (20 m*M* Tris–HCl pH 7.5, 10 m*M* EDTA, 150 m*M* NaCl) at 20:1(*w*:*v*) for an additional two rounds. Inclusion bodies were resuspended in extraction buffer (6 *M* guanidine, 100 m*M* Tris–HCl pH 8.6, 100 m*M* DTT) at 8:1(*w*:*v*) and centrifuged to remove particulates. The denatured extract was refolded by dropwise addition (one drop per second) into a mixing refolding buffer (30 m*M* Tris–HCl pH 9.0, 1 m*M* DTT, 250 m*M* NaCl, 1.2 m*M* GSSG, 0.8 m*M* GSH, 20 µ*M* $ZnSO_4$) at 4°C to obtain a final protein concentration of 0.18 mg $ml^{-1}$. The refolded mixture was pumped onto an XK60 column (GE) containing Ni Sepharose 6 Fast Flow (GE) of 30 mm bed height at a flow rate of 4 ml $min^{-1}$ for a period of 16 h at 4°C, allowing the flowthrough to recycle back onto the column at least two times. The nickel column was washed

**Table 2**
Crystallization.

| | |
|---|---|
| Method | Hanging-drop vapor diffusion |
| Plate type | Neuroprobe 96-well |
| Temperature (K) | 293 |
| Protein concentration (mg ml$^{-1}$) | 14 |
| Buffer composition of protein solution | 20 m*M* Tris–HCl, 100 m*M* NaCl pH 8.0 |
| Composition of reservoir solution | 100 m*M* MMT pH 5, 22.2%(*w*/*v*) PEG 2000 MME |
| Volume and ratio of drop | 0.4 µl:0.4 µl |
| Volume of reservoir (µl) | 500 |

with 10 column volumes (CVs) of IMAC buffer *A* (30 m*M* Tris–HCl pH 7.6, 250 m*M* NaCl, 5 m*M* imidazole) followed by a wash with 10 CVs of 10% IMAC buffer *B* (30 m*M* Tris–HCl pH 7.6, 250 m*M* NaCl, 100 m*M* imidazole). TRAIL was eluted with a linear gradient of 10–100% IMAC buffer *B* over 20 CVs. The eluted fractions were analyzed by SDS–PAGE, pooled, buffer-exchanged into Dulbecco's phosphate-buffered saline (DPBS) and concentrated to 0.6 mg ml$^{-1}$. Verification of proper refolding into a trimer was performed by analysis on an analytical Superdex 200 10/300 GL (GE) column in 20 m*M* sodium phosphate pH 7.2, 200 m*M* NaCl run at 0.5 ml min$^{-1}$.

### 2.2. Preparation of the DR4–TRAIL complex

To prepare the complex, 5.2 mg TRAIL (amino-acid sequence shown in Table 1) was mixed with 24.9 mg DR4 (a fourfold molar excess). This sample was then subjected to dialysis overnight against 20 m*M* Tris–HCl, 100 m*M* NaCl pH 8.0 at 4°C with stirring by employing a 3500 Da cutoff membrane. The following day, the sample was concentrated to 13 ml using Vivaspin 5000 and subjected to size-exclusion chromatography using a 26/60 Superdex 200 column equilibrated with 20 m*M* Tris–HCl, 100 m*M* NaCl pH 8.0.

### 2.3. Crystallization

The purified DR4–TRAIL complex was concentrated to 14 mg ml$^{-1}$ and subjected to crystallization trials. Initial screening used the commercial screens Index, Crystal Screen, Crystral Screen 2 and SaltRx from Hampton Reasearch, Wizard I and II from Emerald Bio, PACT and JCSG+ from Qiagen, OptiMix1, OptiMix2, OptiMix3, OptiMix PEG (4) and OptiMix5 from Fluidigm and two local screens modelled on the commercial screens Natrix/MembFac and Ion Cryo. Optimization around the conditions of the PACT screen with 100 m*M* MMT (1:2:2 ratio of DL-malic acid:MES:Tris base) pH 5.0, 25%(*w*/*v*) PEG 1500 yielded the conditions reported in Table 2.

### 2.4. Data collection and processing

Data were collected on beamline 17-ID at the Advanced Photon Source at Argonne National Laboratory, Argonne, Illinois, USA in July 2009. The data were processed and scaled with *HKL*-2000 (Otwinowski & Minor, 1997) with the resolution and statistics shown in Table 3.

**Table 3**
Data collection and processing.

Values in parentheses are for the outer shell.

| | |
|---|---|
| Diffraction source | 17-ID, APS |
| Wavelength (Å) | 1.0 |
| Temperature (K) | 100 |
| Detector | MAR 165 CCD |
| Crystal-to-detector distance (mm) | 150 |
| Rotation range per image (°) | 1.0 |
| Total rotation range (°) | 180 |
| Exposure time per image (s) | 4 |
| Space group | $P2_12_12_1$ |
| *a*, *b*, *c* (Å) | 84.3, 87.3, 107.1 |
| $\alpha$, $\beta$, $\gamma$ (°) | 90, 90, 90 |
| Mosaicity (°) | 0.4 |
| Resolution range (Å) | 50–3.00 (3.11–3.00) |
| Total No. of reflections† | 122106 (≥10836) |
| No. of unique reflections | 16742 (1639) |
| Completeness (%) | 99.8 (100.0) |
| Multiplicity | 7.3 (7.5) |
| $\langle I/\sigma(I)\rangle$ | 20.8 (6.4) |
| $R_{\rm r.i.m.}$‡ | 0.099 (0.392) |
| Overall *B* factor from Wilson plot (Å$^2$) | 72.7 |

† If any reflections are measured more than four times, then one cannot extract the total number of measured reflections in a shell from the *HKL*-2000 output, but merely a lower limit, hence the use of the '≥' sign. ‡ The redundancy-independent merging *R* factor $R_{\rm r.i.m.}$ has been estimated by multiplying the $R_{\rm merge}$ values by the factor $[N/(N-1)]^{1/2}$, where *N* is the data multiplicity.

**Table 4**
Structure determination and refinement.

Values in parentheses are for the outer shell.

| | |
|---|---|
| Resolution range (Å) | 27.6–3.0 (3.21–3.00) |
| Completeness (%) | 99.8 (100) |
| $\sigma$ Cutoff | 0 |
| No. of reflections, working set | 15492 (2722) |
| No. of reflections, test set | 1049 (206) |
| Final $R_{\rm cryst}$ | 0.173 (0.202) |
| Final $R_{\rm free}$ | 0.225 (0.306) |
| E.s.d. (Luzzati plot) (Å) | 0.3 |
| No. of non-H atoms | |
| Protein | 5676 |
| Ion | 2 |
| Water | 8 |
| Total | 5686 |
| R.m.s. deviations | |
| Bonds (Å) | 0.010 |
| Angles (°) | 1.3 |
| Average *B* factors (Å$^2$) | |
| Protein | 44 |
| Ion | 38 |
| Water | 21 |
| Ramachandran plot† | |
| Most favored (%) | 95.9 |
| Allowed (%) | 99.5 |
| PDB code | 5cir |

† Obtained using *MolProbity* (Chen *et al.*, 2010).

### 2.5. Structure determination and refinement

Molecular replacement used models of TRAIL and DR4 that were derived from the DR5–TRAIL structure (PDB entry 1d0g; Hymowitz *et al.*, 1999). The model of DR5 was modified to reflect the sequence of DR4 by removing side chains that differed. *Phaser* (McCoy *et al.*, 2007) was used for molecular replacement. The TRAIL trimer was placed first, followed by the three DR4 monomers. However, in automated mode *Phaser* could place only two of the three DR4

monomers. Superimposing the 1d0g model of DR5–TRAIL showed that electron density was present along the length of the third DR5 molecule. The third molecule was placed by orienting it as expected from DR5–TRAIL structures and then running the translation function, packing function and refining and phasing, in succession.

*Coot* (Emsley *et al.*, 2010) was used for model building. Refinement was carried out with *autoBUSTER* (Blanc *et al.*, 2004). Display graphics were produced with *PyMOL* v.1.7 (Schrödinger). The buried surface area was calculated with *MS* (Connolly, 1983) using a 1.7 Å probe sphere, contacting residues were enumerated as defined by Sheriff (1993) and Sheriff *et al.* (1987), and both used extended atomic radii as defined by Gelin & Karplus (1979). Structure-refinement statistics are given in Table 4.

### 2.6. Size-exclusion chromatography coupled to multi-angle laser light scattering (SEC-MALS)

Size-exclusion chromatography (SEC) coupled to multi-angle laser light scattering (MALS) was performed using an Agilent 1100 HPLC system (Agilent Technologies) consisting of a Shodex KW-803 column (Phenomenex), a miniDAWN light-scattering detector and an Optilab DSP interferometric refractometer (Wyatt Technology Corporation). Samples were tested at concentrations of 0.4–2.0 mg ml$^{-1}$ (40–60 µg load)

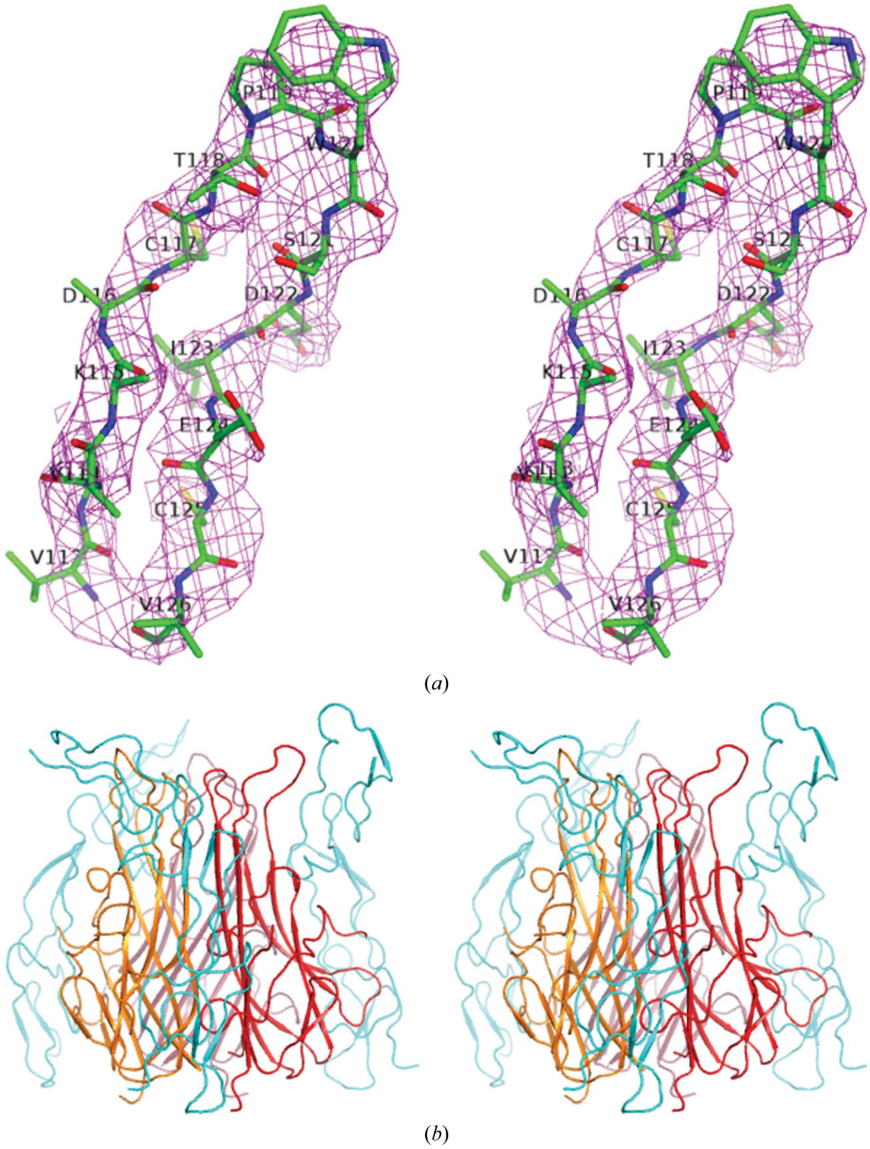


**Figure 1**
Stereo diagrams of (*a*) the residues at the visible C-terminus of DR4, which differ in position from those of DR5 (*d*), with the final $2mF_o - DF_c$ map contoured at 1 r.m.s.d., (*b*) a cartoon diagram of the TRAIL trimer with three DR4 monomers bound as viewed perpendicular to the local threefold, (*c*) a diagram of the TRAIL trimer with three DR4 monomers bound as viewed down the local threefold axis and (*d*) a superposition of the DR5–TRAIL complex (PDB entry 1d0g; cyan) on the DR4–TRAIL complex (red). In (*b*) and (*c*) each monomer of the TRAIL trimer is shown in a different color (red, raspberry and orange) and the DR4 monomers are all shown in cyan. In (*b*) and (*d*) the N-terminal end of both the TRAIL and DR4 chains is at the bottom of the figure and the C-terminal end is at the top. In (*c*) the N-terminal end of the chains is towards the viewer and the C-terminal ends are distal.

**Table 5**
Oligomeric state of the DR4, DR5 and TRAIL proteins.

| Molecule | Monomer predicted molecular mass (kDa) | MALS mass (kDa) | AUC $K_d$† | Solution state‡ |
|---|---|---|---|---|
| DR4 | 15.0 | 14.8 | $>10^{-4}$ *M* | Monomer |
| DR5 | 15.5 | 16.2 | $>10^{-4}$ *M* | Monomer§ |
| TRAIL | 19.6 | 59.2 | $1.5 \times 10^{-13}$ $M^2$¶ | Trimer |

† The monomer/dimer $K_d$ for DR4 and DR5, and the monomer/trimer $K_d$ for TRAIL. ‡ Solution state in the micromolar or higher concentration range, which is the concentration range used in the present study. § Some slight evidence for dimer formation is observed by MALS and AUC. ¶ The equilibrium point between monomer and trimer is $4 \times 10^{-7}$ *M*.

using a mobile phase of 200 m*M* $KH_2PO_4$, 150 m*M* NaCl pH 6.8 at 0.5 ml $min^{-1}$. Data were analyzed using the *ASTRA V* v.5.3.4.16 software (Wyatt Technologies Corporation).

### 2.7. Analytical ultracentrifugation (AUC)

The DR4, DR5 and TRAIL proteins were buffer-matched in phosphate-buffered saline pH 7.1 prior to analysis by analytical ultracentrifugation. Analysis was performed at 20°C using absorbance optics in an XL-I analytical ultracentrifuge using an eight-hole rotor. The partial specific volumes ($\bar{v}$) of each protein were estimated from the amino-acid composition, and the solvent density was estimated from the sum of the density increments of the buffer components using *SEDNTERP* (Laue *et al.*, 1992). Sedimentation-equilibrium analysis was performed using six-channel Epon centerpieces with sapphire windows spinning at 18 000, 25 000 and 33 000 rev $min^{-1}$. Scans were collected at 280 nm and equilibrium was verified by comparing scans at least 6 h apart using the *Match* application, and global nonlinear least-squares fits were performed using *HeteroAnalysis* v.1.1.44.

### 2.8. Microcalorimetry

To prepare the DR4, DR5 and TRAIL proteins for differential scanning calorimetry (DSC) and isothermal titration calorimetry (ITC) studies, each protein was dialyzed into DPBS pH 7.2 (Lonza, catalog No. 17-512Q). For DSC experiments, the samples were subsequently diluted with dialysis buffer to final concentrations of 0.8 mg $ml^{-1}$ DR4, 0.8 mg $ml^{-1}$ DR5 or 0.4 mg $ml^{-1}$ TRAIL, and thermal denaturation was monitored on a MicroCal VP-Capillary DSC instrument using a scan range of 10–110°C and a scan rate of 90°C $h^{-1}$. For ITC studies, samples were diluted with dialysis buffer to concentrations of 80–150 µ*M* DR4 or DR5 and 1.6–4.7 µ*M* TRAIL, and titrations were performed an a MicroCal VP-ITC instrument at 37°C, using 10 µl injection volumes and 20 s duration with an injection spacing of 180 s. All DSC and ITC data were analyzed using *Origin* 7.0 (MicroCal).

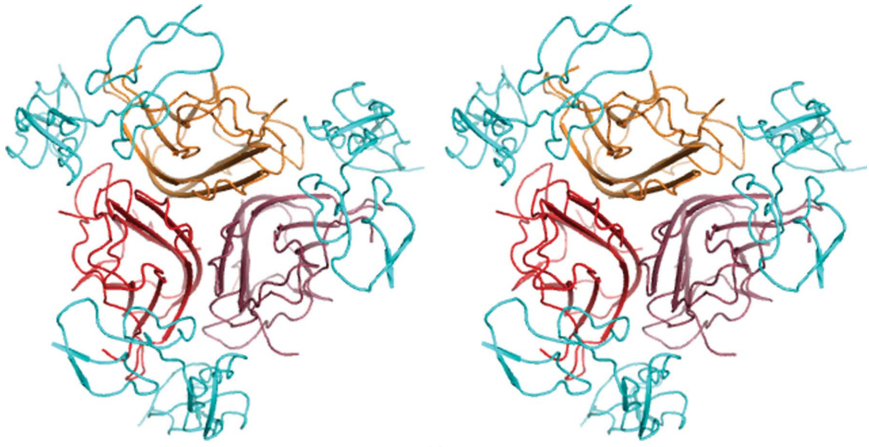

(*c*)

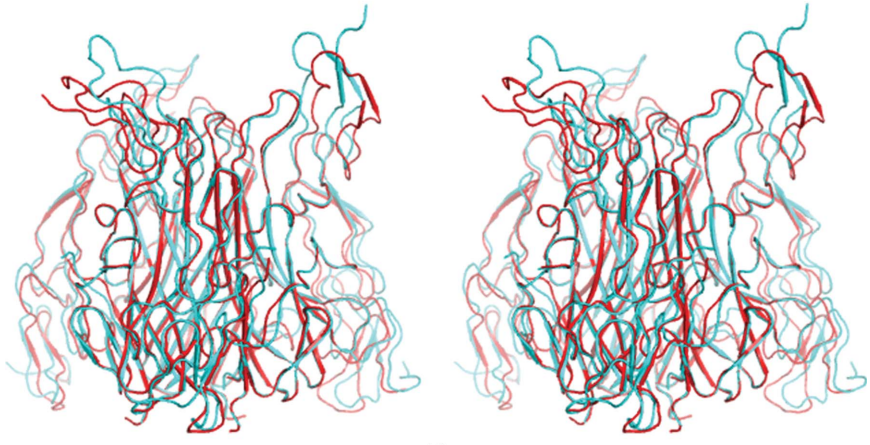

(*d*)

**Figure 1 (continued)**

## 3. Results and discussion

### 3.1. Purification and characterization of DR4, DR5 and TRAIL

His$_6$-tagged DR4 and DR5 as well as untagged TRAIL were expressed in *E. coli* and purified as described in §2. Both the DR4 and DR5 proteins were shown to be monomeric by SEC-MALS and AUC, while the data for TRAIL suggested that the protein forms the expected trimeric structure with a monomer/trimer equilibrium point of 0.4 $\mu M$ and an equilibrium dissociation constant of $1.5 \times 10^{-13}$ $M^2$ in PBS pH 7.1 at 20°C (Table 5).

The chromatogram obtained from the preparation and purification of the DR4–TRAIL complex is shown in Supplementary Fig. S1 and a corresponding gel analysis of the fractions containing the complex is shown in Supplementary Fig. S2.

### 3.2. Overall structure of the DR4–TRAIL complex

Differences in the trace of parts of DR4 compared with DR5 were obvious and the final map shows good electron density (Fig. 1*a*). As previously noted, TRAIL consists of $\beta$-sandwiches with a jelly-roll topology (Hymowitz *et al.*, 1999;

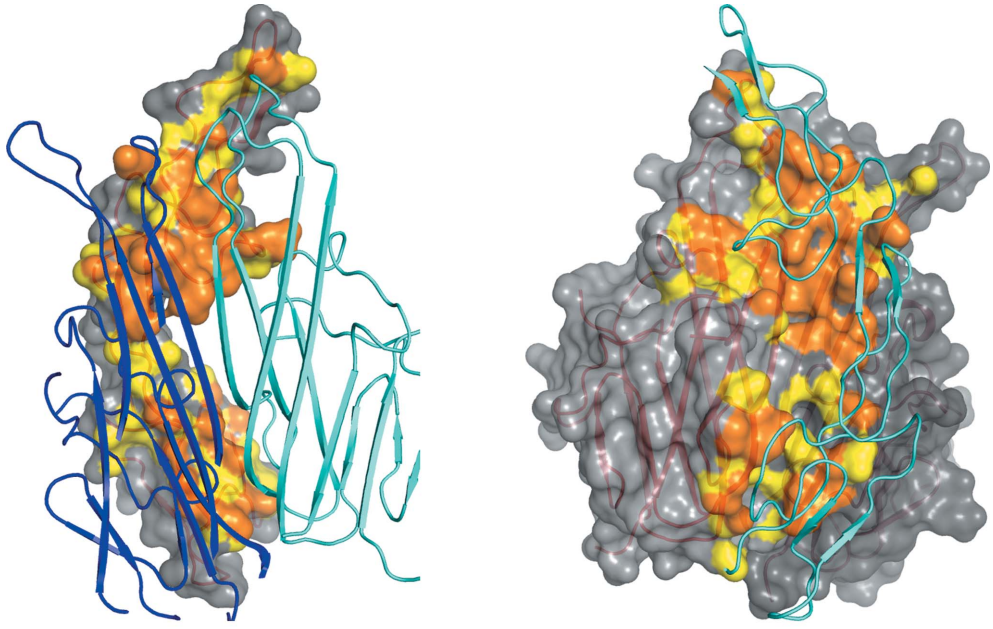


**Figure 2**
DR4–TRAIL complex interactions. (*a*) Surface representation of DR4 (contacting residues, orange; buried residues, yellow; non-interacting residues, gray) with the two monomers of TRAIL that interact with this monomer shown as cartoons. (*b*) Surface representation of TRAIL (contacting residues, orange; buried residues, yellow; non-interacting residues, gray) with DR4. (*c*) Sequence comparison of the DR4 and DR5 sequences, with identical residues in red. (*d*, *e*) Surface representations of DR4 and DR5 (contacting residues, orange; buried residues, yellow; non-interacting residues, gray) showing the similarity of interactions. (*f*) DR4 and DR5 interactions with TRAIL in the vicinity of TRAIL residues 191 and 267–169, showing that the replacement of an Asp-Ser-Gly sequence in DR5 by a Lys-Ser-Asp sequence in DR4 leads to different local interactions, while maintaining the overall interactions between the two proteins.

Mongkolsapaya *et al.*, 1999). A total of three DR4 molecules are bound to the TRAIL trimer, with each DR4 binding to two adjacent TRAIL monomers in the trimer (Figs. 1*b* and 1*c*).

The overall structure of the DR4–TRAIL complex is very similar to that of the DR5–TRAIL complex (Fig. 1*d*). The structure of the TRAIL trimer in the complex is in most aspects extremely similar to those of TRAIL in the three reported complexes with DR5 (PDB entries 1d0g, 1d4v and 1du3; Hymowitz *et al.*, 1999; Mongkolsapaya *et al.*, 1999; Cha *et al.*, 2000) and apo TRAIL (PDB entry 1dg6; Hymowitz *et al.*, 2000). Major differences are confined to loop regions that are not involved in interactions with receptors, *e.g.* 129–131, which is adjacent to a large unstructured stretch in the apo structure and all of the complexes except 1d4v, 156–160 and 198–200, which are both loops and differ amongst all of the structures. Although $Zn^{2+}$ was not added to the crystallization buffer, a $Zn^{2+}$ site was found at the same location as seen in apo TRAIL (PDB entry 1d6g) and two of the complexes with DR5 (PDB entries 1d0g and 1du3), and was presumably acquired during protein expression. This leads to a difference near residues 230–234, which is a loop near the $Zn^{2+}$-binding site and is different only in PDB entry 1d4v, which does not have $Zn^{2+}$ bound. Fig. 1(*d*) gives the impression that DR4 is farther away from TRAIL at both the N- and C-termini than DR5 is from TRAIL. However, direct superposition of DR5 on DR4 shows that while the termini and a few loops are in different places, the bulk of the structure traces the same path.

Like DR5 and other members of the TNF receptor family, the DR4 structure consists of at least three cysteine-rich domains (CRD) that form an extended structure. The cysteine-rich domains are held together principally by two or three disulfide bonds. TNF receptors have very little in the way of secondary structure beyond, perhaps, a pair of three-residue $\beta$-strands in each CRD. Unsurprisingly, DR4 and DR5, which are 60% identical, are structurally very similar, but other TNF receptors with more divergent sequences maintain this same structure, presumably owing to the retention of cysteines and disulfide bonds. Naismith & Sprang (1998), building on a suggestion by Bazan (1993), propose that rather than considering the CRDs as monolithic they actually consist of modules that have either one or two disulfide bonds and typically one of two different folds identified as A and B, yielding modules of the form A1, A2, B1, B2, where the number identifies the number of disulfide bonds and where a CRD typically consists of an A and a B module. According to Table 1 of Naismith & Sprang (1998), they predict on the basis of sequence for DR4 that it will have a module structure of A1–A2–B2–A1–B2. We find a module structure of A1–A1–B2–A1–B2 (Supplementary Table S1). Since the module that Naismith and Sprang identify as A2 has only one disulfide bond, we suspect a typographical error. DR5 has an identical pattern to DR4, although Cha *et al.* (2000) refer to the first module as N1.

The interactions between DR4 and TRAIL are summarized in Supplementary Tables S2 and S3, respectively, as averages for the three DR4 monomers and the TRAIL trimer. Figs. 2(*a*) and 2(*b*) show the interaction surfaces of DR4 and TRAIL, respectively, with the contacting surface in orange and the buried surface in yellow. The interaction surfaces of both proteins are relatively large at ∼1130 Å$^2$ for each protein. A sequence alignment of DR4 *versus* DR5 is shown in Fig. 2(*c*), which shows that the segments of interaction with TRAIL are not completely conserved. Nevertheless, comparison of the interaction surfaces of DR4 in this complex (Fig. 2*d*) with that of one of the monomers in the DR5–TRAIL complex with PDB code 1d0g (Fig. 2*e*) shows considerable congruence. However, one example of where different sequences lead to different specific interactions while maintaining the overall

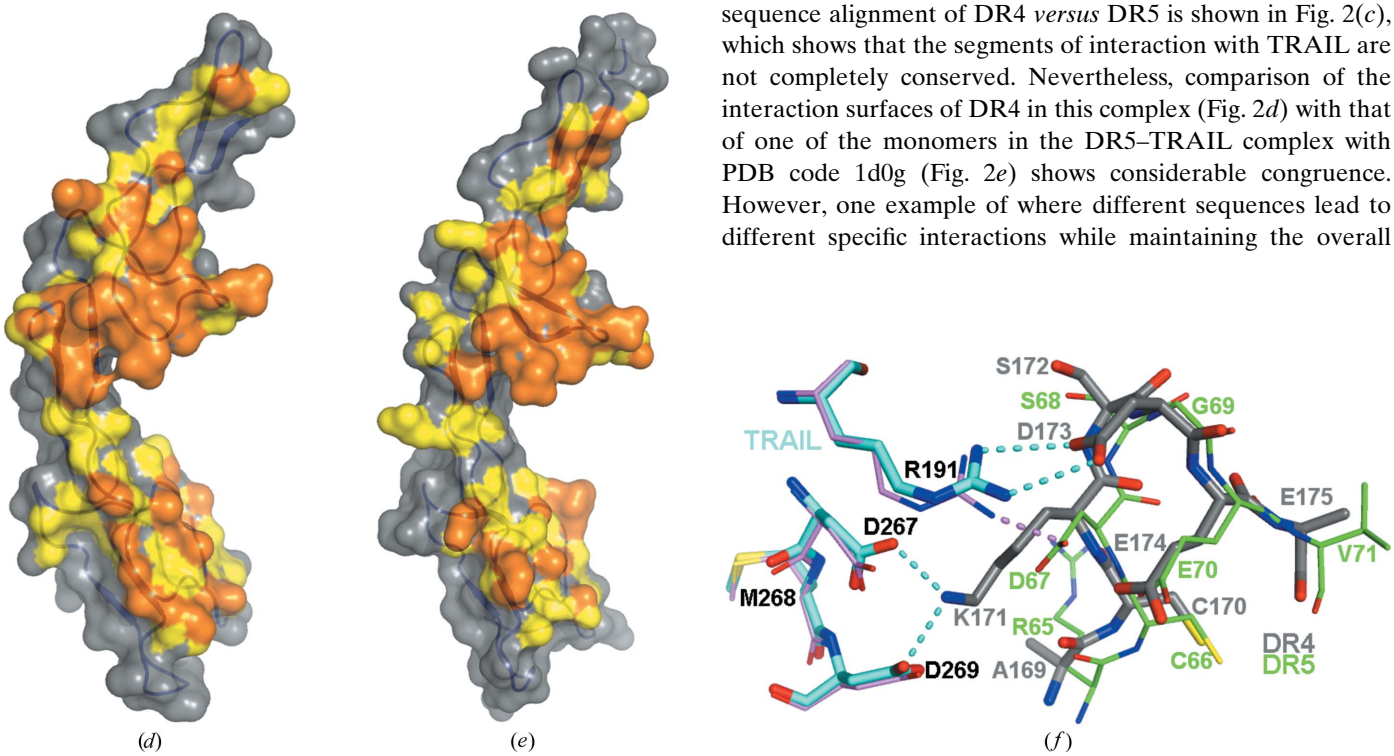


(*d*) (*e*) (*f*)

**Figure 2 (continued)**

interaction is shown in Fig. 2(*f*), where an Asp-Ser-Gly (120–122) sequence in DR5 is replaced by a Lys-Ser-Asp (171–173) sequence in DR4. The Lys in DR4 interacts with two Asp residues in TRAIL that are not engaged in interactions in the DR5–TRAIL complex. However, although at opposite ends of the sequence triad, the two Asp residues in the DR5 and DR4 structures interact with the same Arg191.

### 3.3. Specific differences between DR4–TRAIL and DR5–TRAIL

Given the high sequence similarity between DR4 and DR5, most of the differences in their interaction with TRAIL are subtle. However, Fig. 2(*f*) shows a region where amino-acid changes do impact the arrangement of hydrogen bonds and salt links between DR4/DR5 and TRAIL. Specifically, Asp120 of DR5 forms a salt link with Arg191 of TRAIL, whereas Lys171 of DR4 extends farther and forms salt links with Asp267 and Asp269 of TRAIL. The lost salt link in the DR5–TRAIL complex is replaced by the formation of a bidentate salt link between Asp173 of DR4 and Arg191 of TRAIL.

### 3.4. Thermodynamic differences in DR4–TRAIL compared with DR5–TRAIL interactions

To determine whether the structural differences between the DR4–TRAIL and DR5–TRAIL complexes translate into detectable differences in the thermodynamics of the binding interactions, we performed ITC studies of DR4 or DR5 titrated into TRAIL at 37°C. Consistent with earlier ITC studies using bivalent DR4-Fc or DR5-Fc fusion proteins (Truneh *et al.*, 2000), we found that the enthalpy of TRAIL binding was significantly larger for DR4 compared with DR5 (Fig. 3). Moreover, the shapes of the binding isotherms were significantly different from each other. The DR4 binding curve consists of at least two distinct binding phases: the first with higher affinity ($K_d$ = ~$10^{-8}$ *M*) and a larger enthalpy and the second with lower affinity ($K_d$ = ~$10^{-6}$ *M*) and a smaller

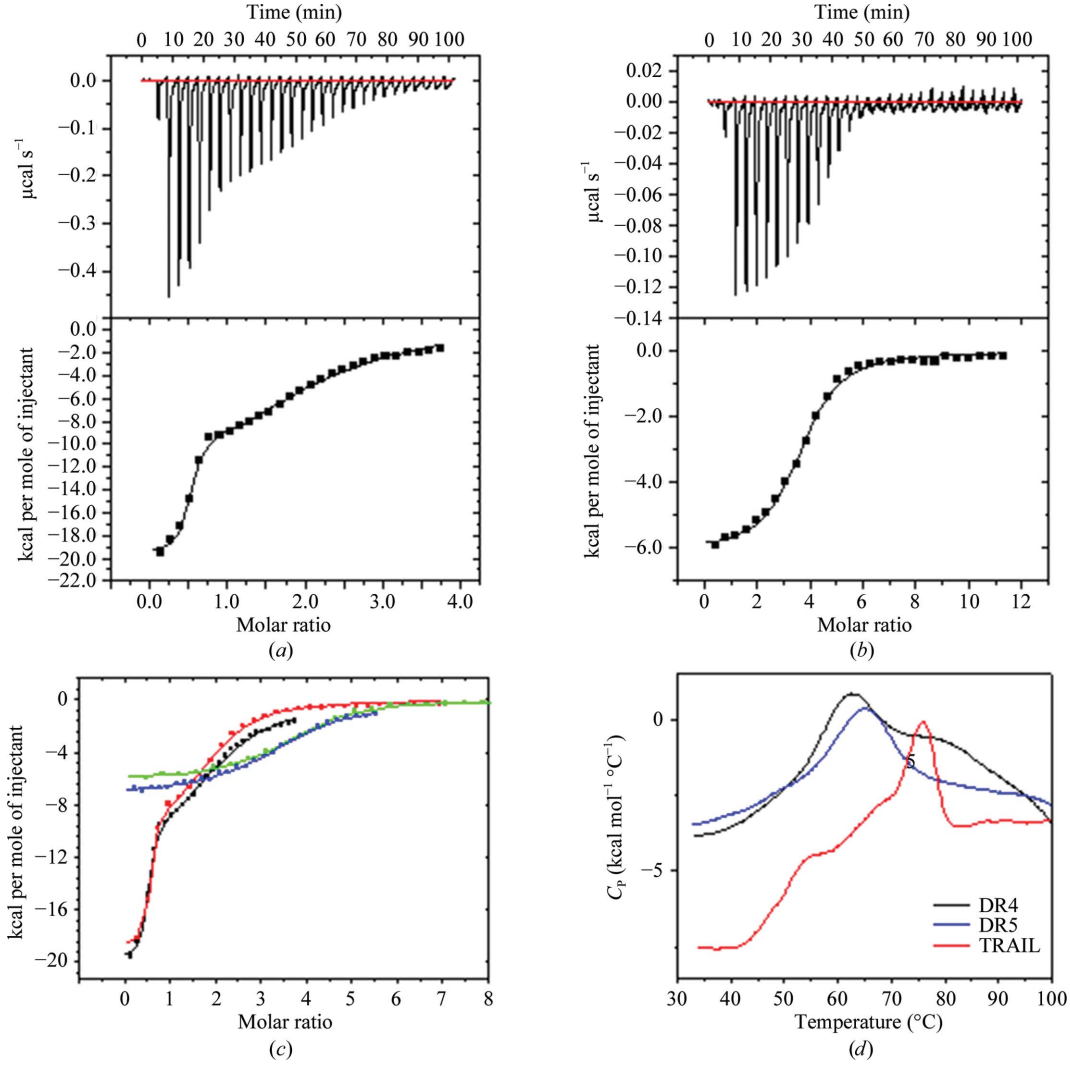


**Figure 3**
Isothermal titration calorimetry data for DR4 or DR5 binding to TRAIL. (*a*) 80 µ*M* DR4 titrated into 4.7 µ*M* TRAIL. (*b*) 80 µ*M* DR5 titrated into 1.6 µ*M* TRAIL. (*c*) Overlay of ITC binding isotherms for titrations of 80 µ*M* DR4 *versus* 4.7 µ*M* TRAIL (black), 150 µ*M* DR4 *versus* 4.7 µ*M* TRAIL (red), 80 µ*M* DR5 *versus* 3.1 µ*M* TRAIL (blue) and 80 µ*M* DR5 *versus* 1.6 µ*M* TRAIL (green). (*d*) Differential scanning calorimetry thermograms showing the thermal denaturation of DR4 (black), DR5 (blue) and TRAIL (red).

enthalpy (Fig. 3*a*). In contrast, the DR5 binding curve is well described by a homogeneous set of binding sites model with intermediate affinity ($K_d$ = $\sim 10^{-7}$ *M*; Fig. 3*b*). Therefore, despite the structural similarity between the complexes of DR4–TRAIL and DR5–TRAIL described above, the ITC data show clear thermodynamic differences in the binding interactions.

The homogeneity of the DR5–TRAIL ITC binding curves is consistent with a simple binding mechanism, and also demonstrates the functional homogeneity and high quality of both the DR5 and TRAIL reagents. To further investigate the multiphasic nature of the DR4–TRAIL interactions, we performed DSC studies for each protein in the same PBS buffer and at similar protein concentrations to those at which the ITC studies were performed. Under these conditions, DR4, DR5 and TRAIL were each shown to have melting transitions well above the temperature at which the ITC studies were performed (>37°C), confirming that the ITC was probing interactions of folded conformations of each protein. The DSC data for DR5 consisted of a single transition with a denaturation midpoint temperature ($T_m$) of 65°C. The DSC data for DR4 showed a similar transition with $T_m$ = 63°C, but also showed a minor transition followed by a downward-sloping baseline at higher temperatures characteristic of aggregation of the denatured form (Fig. 3*d*). Interestingly, although TRAIL was shown to be a stable trimer by both MALS and AUC (Table 2) at 25°C, the DSC data for TRAIL showed the presence of three overlapping transitions with $T_m$ values of ∼53, ∼67 and ∼76°C, suggesting the presence of subpopulations with different thermal stabilities under these conditions (Fig. 3*d*). The thermodynamic differences in binding observed by ITC may indicate that DR5 binds TRAIL with uniform stepwise binding, whereas DR4 may interact with TRAIL in a more complex manner.

## 4. Discussion

We report the first structure of a DR4–TRAIL complex, which is also the first structure of DR4. The DR4–TRAIL structure is very similar overall to that of DR5–TRAIL, and the structure of DR4 is very similar to that of DR5. However, some differences do exist that are the result of sequence differences between DR5 and DR4. Interestingly, the structural differences are accompanied by clear differences in the thermodynamics of binding of DR4 or DR5 to TRAIL. In other studies (Truneh *et al.*, 2000; Reis *et al.*, 2011) differences in binding have been observed, but binding is often reported as being complex and most reports have tested the binding of DR4-Fc or DR5-Fc fusion proteins to TRAIL. Thus, further experiments would be necessary to better characterize and understand these differences and determine how they relate to the different biological activities of DR4 and DR5. The structures of the DR4–TRAIL and DR5–TRAIL complexes do not shed light on how TRAIL mutants, *e.g.* S159R (Yu *et al.*, 2014), impart selectivity for DR4 over DR5, as none of the residues described are involved with either DR4 or DR5. At this state of our knowledge, it is unclear from structural and biophysical studies why two receptors are necessary. However, these data may provide sufficient information for the design of specific antagonists or agonists in the manner described for LIGHT with decoy receptor 3 (Dcr3) by Liu *et al.* (2014).

## Acknowledgements

Use of the Advanced Photon Source was supported by the US Department of Energy, Office of Science, Office of Basic Energy Sciences under Contract No. DE-AC02-06CH11357 and use of the IMCA-CAT beamline 17-ID at the Advanced Photon Source was supported by the companies of the Industrial Macromolecular Crystallography Association through a contract with Hauptman–Woodward Medical Research Institute. We thank Shamrock Structures for collecting the data.

## References

Bazan, J. F. (1993). *Curr. Biol.* **3**, 603–606.
Blanc, E., Roversi, P., Vonrhein, C., Flensburg, C., Lea, S. M. & Bricogne, G. (2004). *Acta Cryst.* D**60**, 2210–2221.
Cha, S.-S., Sung, B.-J., Kim, Y.-A., Song, Y.-L., Kim, H.-J., Kim, S., Lee, M.-S. & Oh, B.-H. (2000). *J. Biol. Chem.* **275**, 31171–31177.
Chen, V. B., Arendall, W. B., Headd, J. J., Keedy, D. A., Immormino, R. M., Kapral, G. J., Murray, L. W., Richardson, J. S. & Richardson, D. C. (2010). *Acta Cryst.* D**66**, 12–21.
Connolly, M. L. (1983). *J. Appl. Cryst.* **16**, 548–558.
Emsley, P., Lohkamp, B., Scott, W. G. & Cowtan, K. (2010). *Acta Cryst.* D**66**, 486–501.
Gelin, B. R. & Karplus, M. (1979). *Biochemistry*, **18**, 1256–1268.
Hymowitz, S. G., Christinger, H. W., Fuh, G., Ultsch, M., O'Connell, M., Kelley, R. F., Ashkenazi, A. & de Vos, A. M. (1999). *Mol. Cell*, **4**, 563–571.
Hymowitz, S. G., O'Connell, M. P., Ultsch, M. H., Hurst, A., Totpal, K., Ashkenazi, A., de Vos, A. M. & Kelley, R. F. (2000). *Biochemistry*, **39**, 633–640.
Laue, T. M., Shah, B. D., Ridgeway, T. M. & Pelletier, S. L. (1992). *Analytical Ultracentrifugation in Biochemistry and Polymer Science*, pp. 90–125. Cambridge: The Royal Society of Chemistry.
Liu, W., Zhan, C., Cheng, H., Kumar, P. R., Bonanno, J. B., Nathenson, S. G. & Almo, S. C. (2014). *Structure*, **22**, 1252–1262.
McCoy, A. J., Grosse-Kunstleve, R. W., Adams, P. D., Winn, M. D., Storoni, L. C. & Read, R. J. (2007). *J. Appl. Cryst.* **40**, 658–674.
Mongkolsapaya, J., Grimes, J. M., Chen, N., Xu, X.-N., Stuart, D. I., Jones, E. Y. & Screaton, G. R. (1999). *Nature Struct. Biol.* **6**, 1048–1053.
Naismith, J. H. & Sprang, S. R. (1998). *Trends Biochem. Sci.* **23**, 74–79.
Otwinowski, Z. & Minor, W. (1997). *Methods Enzymol.* **276**, 307–326.
Prasad, S., Kim, J. H., Gupta, S. C. & Aggarwal, B. B. (2014). *Trends Pharmacol. Sci.* **35**, 520–536.
Reis, C. R., van Assen, A. H., Quax, W. J. & Cool, R. H. (2011). *Mol. Cell. Proteomics*, **10**, M110.002808.
Roosmalen, I. A. M. van, Quax, W. J. & Kruyt, F. A. E. (2014). *Biochem. Pharmacol.* **91**, 447–456.
Sheriff, S. (1993). *Immunomethods*, **3**, 191–196.
Sheriff, S., Hendrickson, W. A. & Smith, J. L. (1987). *J. Mol. Biol.* **197**, 273–296.
Stuckey, D. W. & Shah, K. (2013). *Trends Mol. Med.* **19**, 586–594.
Truneh, A., Sharma, S., Silverman, C., Khandekar, S., Reddy, M. P., Deen, K. C., Mclaughlin, M. M., Srinivasula, S. M., Livi, G. P., Marshall, L. A., Alnemri, E. S., Williams, W. V. & Doyle, M. L. (2000). *J. Biol. Chem.* **275**, 23319–23325.
Yu, R., Albarenque, S. M., Cool, R., Quax, W. J., Mohr, A. & Zwacka, R. M. (2014). *Cancer Biol. Ther.* **15**, 1658–1666.